Computers & Structures Vol. 31, No. 1, pp. 81–92, 1989
Printed in Great Britain.

0045-7949/89 $3.00 + 0.00
Pergamon Press plc

SOME RECENT APPLICATIONS OF NUMERICAL METHODS TO GEOTECHNICAL ANALYSIS

J. R. BOOKER, J. P. CARTER, J. C. SMALL, P. T. BROWN and H. G. POULOS
School of Civil and Mining Engineering, University of Sydney, NSW 2006, Australia

Abstract—In geotechnical engineering it is often important to take into account construction path, constitutive modelling and three-dimensional effects. In such cases the use of the most complicated form of analysis may not be feasible and it is necessary to adopt simpler approaches which recognise the most important geotechnical aspects of the situation.

INTRODUCTION

The finite element method has gained wide acceptance amongst geotechnical engineers as a valuable method of analysis. It has the great advantage of being able to model the complex geometrical features and the wide variety of materials which occur in the geotechnical context as well as being able to incorporate when necessary the complex constitutive behaviour that characterizes real soil and rock.

An awareness of these advantages has been reflected in the literature which reports on many applications of the finite element method to highly realistic problems. There is clear evidence that many geotechnical analysts are conscious of the possibility of discretization error and problems associated with round-off error in the solution of large sets of linear equations.

It is, however, not always appreciated that in order to model a given situation realistically it is often necessary to model the actual construction sequence. In such cases it is not always evident what constitutes an adequate approximation. Similarly, no single constitutive model adequately models all facets of real soil or rock behaviour and even if such a model did exist its incorporation, in full complexity, in a finite element analysis might prove prohibitively costly. It is consequently necessary to adopt a simplified model and to determine the physical parameters associated with the model by tests which reflect the in-ground stress path as closely as possible. Finally, sometimes, particularly in three-dimensional analysis, the straightforward application of the finite element method leads to an extremely large set of approximating equations which cannot be solved economically. In such cases it is necessary to adopt an alternative strategy.

In this paper the matters mentioned in the previous paragraph will be discussed and illustrated. Both finite element and boundary element methods will be discussed. Attention will be restricted to geotechnical applications and illustrations will be drawn predominantly from the authors' research.

FINITE ELEMENT APPROACHES

Analysis of excavation

The finite element method has often been used to simulate excavation. When the soil is linearly elastic, the results of excavation should be independent of the number of stages in the excavation process, and lack of such independence indicates an incorrect procedure. A method whose errors do not increase with the number of stages of excavation is a necessary basis for multi-stage excavation is non-linear problems.

Simulation of excavation involves determination of the nodal force equivalents of the tractions at the new portion of the solid boundary, and this may be carried out by a variety of methods. Christian and Wong [1] considered methods involving direct determination of tractions and nodal forces from known values of stress and report a variety of disturbing effects.

A direct method [2], based on the virtual work equation including the terms due to stresses, body forces and external tractions, is simpler to implement than stress extrapolation, and gives results which are independent of the number of stages of excavation, without the need for special care. The virtual work equation leads directly to the following finite element equation for the increment of deflections Δa:

$$\int_V (B^T D B)\,\mathrm{d}V \Delta a = -\int_V (B^T \sigma)\,\mathrm{d}V + \int_V (N^T \gamma)\,\mathrm{d}V + \int_S (N^T t)\,\mathrm{d}S$$

where V, S, γ and t denote the current volume, surface, body force and applied tractions and σ denotes the stress state immediately prior to the current increment of excavation as shown in Fig. 1.

At times, other investigators have evaluated the nodal forces by ignoring the contribution from the body forces, and ignoring the nodal forces which then arise at nodes other than on the current excavated

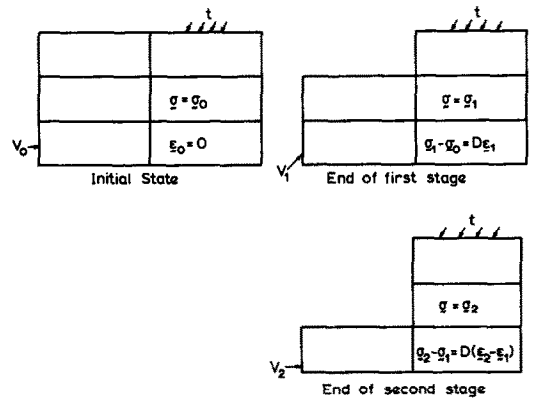

Fig. 1. Schematic excavation process.

boundary. In this way a reasonably satisfactory solution can be obtained, as shown in Fig. 2, although it may be seen that serious errors occur near the top of the cut. However with very little more trouble it would have been possible to obtain a correct solution by the method described.

Integral transform techniques

Frequently geotechnical engineers are called upon to determine the elastic response of a prismatic body (two-dimensional geometry) which is subject to three-dimensional loading. For example, it may be necessary to analyse the effect of a building being constructed above an existing tunnel (see Fig. 3).

In such cases the analysis can be simplified by the introduction of a Fourier transform

$$U = \frac{1}{2\pi}\int_{-\infty}^{\infty} u e^{-i\alpha z}\,dz \tag{1a}$$

with the inverse transform

$$u = \int_{-\infty}^{\infty} U e^{+i\alpha z}\,d\alpha. \tag{1b}$$

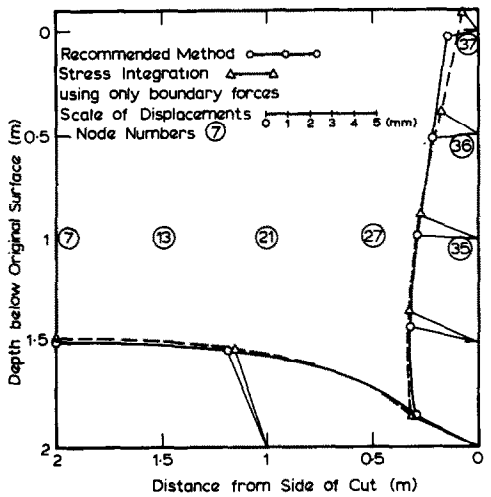

Fig. 2. Displacements at end of excavation.

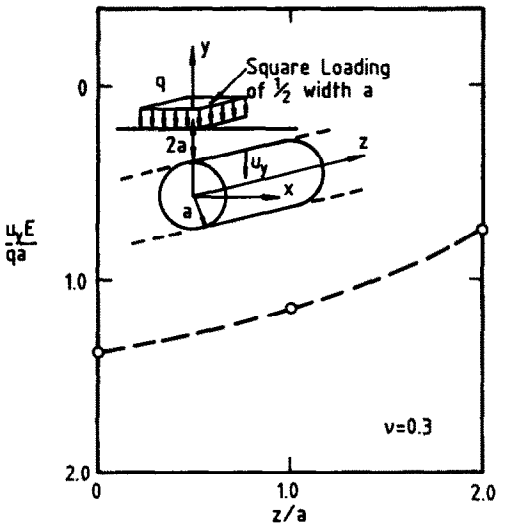

Fig. 3. Displacement of tunnel roof.

Application of such transforms to the equations of elasticity removes dependence on the z coordinate, thus reducing the problem from a three-dimensional one to a two-dimensional in the transformed variables.

In order to establish a finite element approximation we take the equation of virtual work, which in the absence of body forces

$$\int_V d\epsilon^T \sigma\,dV = \int_S du^T t\,dS. \tag{2}$$

We observe that the displacement field $\mathbf{u} = \mathbf{U}(x, y, \alpha)e^{i\alpha z}$, satisfies the equations of elasticity with surface tractions $\mathbf{t} = \mathbf{T}(x, y, \alpha)e^{i\alpha z}$ and induced strains $\epsilon = \mathbf{E}(x, y, \alpha)e^{i\alpha z}$.

If we approximate the transformed nodal variables and determine stress and strain in the usual way, viz.

$$\mathbf{U} = \mathbf{N}\Lambda \tag{3a}$$

$$\mathbf{E} = \mathbf{B}\Delta \tag{3b}$$

where Δ is the vector of nodal values of $\mathbf{U}$, $\mathbf{N}$ is the matrix of shape or interpolation functions, $\mathbf{B}$ is the strain–displacement matrix.

Substitution of eqns (3) into the virtual work eqn (2) leads to the set of transformed stiffness equations

$$\mathbf{K}\Delta = \mathbf{F} \tag{4}$$

where

$$\mathbf{K} = \int \mathbf{B}^T\mathbf{D}\mathbf{B}\,dV$$

$$\mathbf{F} = \int \mathbf{N}^T\mathbf{T}\,dS.$$

The solution of eqn (3) will provide values of the quantity Δ which are in effect the transformed values of the displacements at the nodes of the elements. These must firstly be inverted to obtain the final solution for the displacements at the nodes δ, e.g.

$$\delta = \int_{-\infty}^{+\infty} \Delta e^{+i\alpha z} \, d\alpha. \tag{5}$$

The integral of eqn (5) is best evaluated by using numerical integration and in this paper, Gaussian quadrature was selected. We have therefore

$$\delta = \sum_{j=i}^{N} W_j \Delta(\alpha_j) e^{+i\alpha_j z} \tag{6}$$

where W_j are the Gaussian weights and α_j are the Gaussian coordinates. To do this we must truncate the infinite limits of the integral of eqn (5) at some finite value which is large enough so that the numerical integration of eqn (6) closely approximates the correct result.

Hence we may set up and solve the set of eqns (4) for a particular value of α_j and solve to obtain a value of Δ. By carrying out the summation shown in eqn (6) we can invert the solution to obtain the displacements at any z coordinate.

As an example, the problem of a structure being built over an existing tunnel is analysed. This problem is shown schematically in the inset to Fig. 3. It is of interest to be able to calculate the stress increases caused around the tunnel, and to be able to predict the length of tunnel (in the z direction) which will be effected by the structure. In the example given here, the stresses evaluated are the changes caused by the weight of the structure, and do not include the initial stresses which exist around the tunnel after excavation.

Figure 3 also shows a plot of the non-dimensionalized vertical displacement $u_y E/qa$ (E is the modulus of the soil, q is the applied loading, a is the radius of the tunnel, u_y is the vertical deflection) of the roof of the tunnel at different distances from the centerline of the loading. The influence of the loading on the tunnel may be seen to be quite considerable even at a distance $z/a = 2$ where the vertical deflection is slightly more than 50% of that at the centreline.

Plots of stress contours on planes perpendicular to the axis of the tunnel (i.e. x–y planes) are shown in Fig. 4. Contours of non-dimensional vertical stress σ_{yy}/q are plotted on the planes at $z/a = 1$ and $z/a = 2$. The stress field may be seen to change substantially between these two planes near the surface; however, around the tunnel, stresses are generally of the same magnitude.

Finite layer theory

In the previous example Fourier transforms were applied to full three-dimensional problems in order to reduce the problem to one involving only two spatial dimensions. This idea may be extended further if the problem to be solved is such that the boundary conditions and the material properties do not vary in two axis directions. We may apply a double Fourier transform to reduce the problem to one involving a single spatial dimension only.

Example

As an example of the application of Fourier transform techniques to stress analysis problems, the problem of a strip, circular or rectangular loading applied to a soil layer is analysed. In the case of a strip loading, only a single Fourier transform is needed; for a rectangular loading a double Fourier transform is used, and for a circular loaded region a Hankel transform is used as it may be shown that a double Fourier transform becomes a Hankel transform in this case. The three different loading problems are shown schematically in the inset to Fig. 5b.

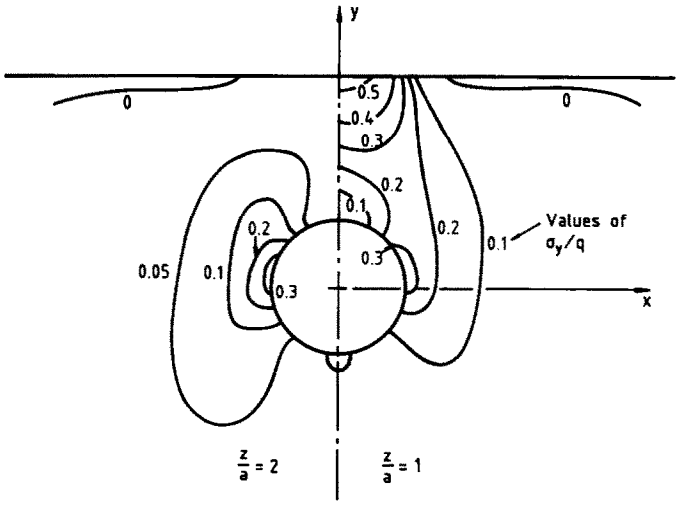

Fig. 4. Vertical stress contours.

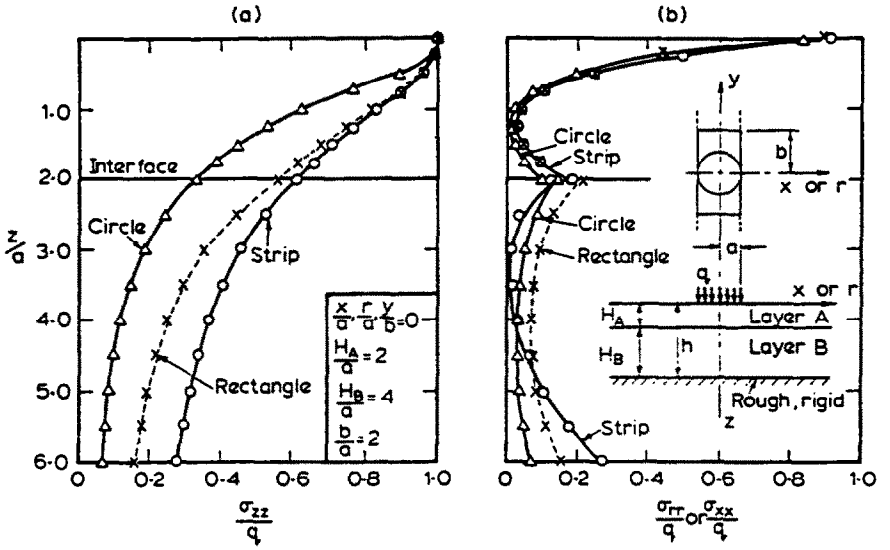

Fig. 5. Stresses in layered material.

Dimensions of the loaded areas and of the material layers A and B are given in Fig. 5a.

Each of the material layers is chosen to be cross-anisotropic with properties as given in Table 1.

Vertical stress σ_{zz} and horizontal stress σ_{rr} (circle) or σ_{xx} (strip, rectangle) are plotted along the centreline $x = y = 0$ or $r = 0$ in normalized form σ/q in Fig. 5a,b (q is the uniform applied loading). It may be seen that there is a large variation in vertical stress for the different loading shapes (Fig. 5a). Horizontal stresses are also different, especially in layer B, and show a discontinuity across the layer interface where it is assumed that no slip occurs. The analysis was performed using program FLEA [3] and took 33 sec on an IBM-PC with an 8087 coprocessor.

Problems involving consolidation of a layered soil stratum may also be solved using this technique. Once again the problem of a circular loading is used to demonstrate the method. This loading q is applied to the surface of a soil stratum consisting of two layers of equal thickness; this is shown schematically in inset (i) to Fig. 6a.

The material properties of the layers (which are isotropic) are such that the ratio of the shear moduli is $G_A/G_B = 1/4$ and the ratio of the permeabilities is $k_A/k_B = 4$ (the subscripts A, B refer to the layers as shown in Fig. 6a).

Table 1.

	Layer A	Layer B
E_h/E_v	1.5	3.0
$2G_v/E_v$	0.9	1.0
ν_h	0.25	0.1
ν_{vh}	0.2	0.3

E_h, E_v are the moduli of elasticity in the horizontal and vertical directions respectively. ν_h, ν_{vh} are the Poisson's ratio giving the effect of horizontal strain on complementary horizontal strain and vertical strain on horizontal strain. G_v is the independent shear modulus of the material.

With this type of analysis, one-dimensional elements are used as shown in inset (ii) to Fig. 6a and accuracy depends upon the type of discretization used. Accuracy also depends upon the amount of numerical integration used to invert the transformed field variables. For the example given here Gaussian integration was used, and this involved obtaining solutions at 80 Gauss points using a 20 point Gaussian quadrature scheme.

Values computed for the vertical settlement w at the central point of the loaded area are plotted in non-dimensional form $G_A w/qa$ against non-dimensional time τ in Fig. 6a (the quantity τ is defined on the figure where γ_w is the unit weight of water).

Figure 6b shows the distribution of excess pore pressure p along the centreline $r = 0$ of the loading. Initially (i.e. at small values of τ) these pore pressures are higher in the upper layer than the lower layer, but as the upper surface of the soil stratum is more permeable, these pore pressures quickly dissipate leaving the higher pressures in the lower layer. The analysis was performed using program FLAC [4] and ran for 8 min 26 sec on an IBM-PC with an 8087 coprocessor.

BOUNDARY ELEMENT APPROACHES

Many problems which are truly three-dimensional in nature are not amenable to finite element analysis because of computer storage requirements, computational costs or problems of numerical accuracy. For an elastic material many of these problems can be overcome by the use of boundary element methods.

In order to illustrate the use of boundary elements combined with a proper attention to details of load path we shall investigate the analysis of an underground excavation aided by a support system.

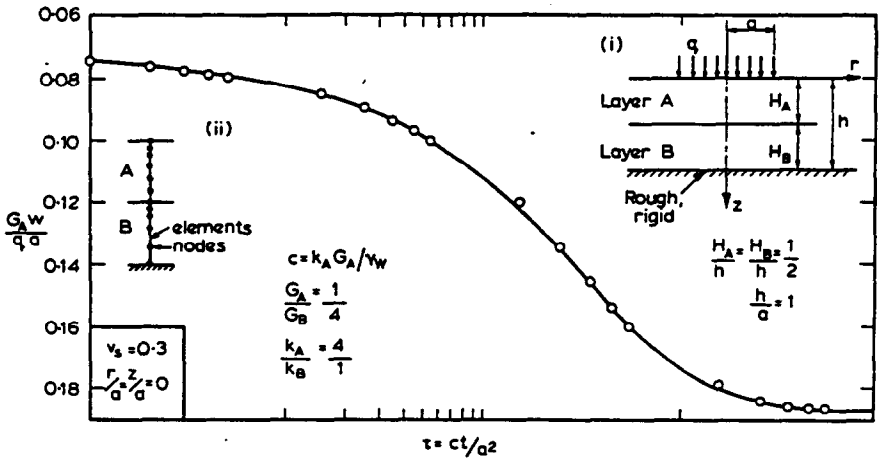

Fig. 6a. Time settlement of circular footing.

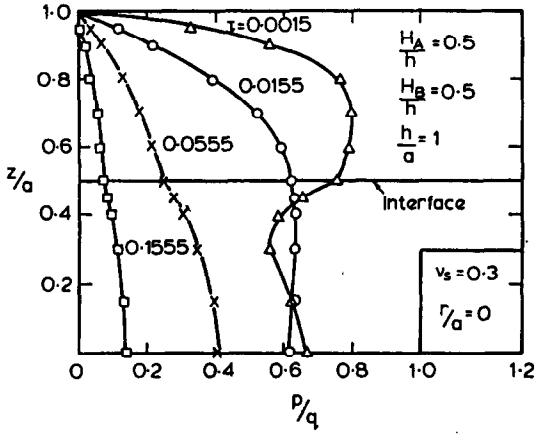

Fig. 6b. Pore pressure isochrones.

Longwall support

The longwall method of mining is used in many collieries to extract coal from tabular seams. The technique involves the use of a moveable coal cutter, conveyor and roof support system. A schematic illustration of a typical longwall layout is given in Fig. 7. In practice the moveable supports commonly are powered hydraulically and will yield vertically at a pre-set maximum axial load.

An important problem for designers of longwall supports is to predict reliably the loads tramsmitted to the supports as coal is extracted from the seam and the coal face advances, creating an increasingly large underground opening. One means of making such predictions involves the analysis of the structural interaction between the supports and the surrounding rock mass, including the changing nature of that interaction as the face advances. A suitable method for analysis is the boundary element or finite element technique. The former of these procedures is discussed below.

Idealizations

To ensure that the problem remains tractable a number of idealizations are required. The idealization of the problem geometry is indicated in Fig. 8, which shows the assumed initial condition and the configuration at two consecutive stages, i and $i + 1$, of the extraction.

The length of the longwall face w is large so that it may reasonably be assumed that conditions of plane strain apply along most of the length of the face, i.e. movement of the rock mass will occur in vertical planes which are aligned along the direction of advance of the face, and thus there is no component of movement perpendicular to this direction.

The coal seam is assumed to be horizontal and of uniform thickness t. The width of the extracted section is assumed to reach a maximum unsupported span of l_0 after which the support system is installed. It is assumed that the face then advances in finite increments by extraction of a width e of coal from the face. The support system is assumed to move at the same time as the coal is removed incrementally from the face so that it always remains a constant distance d from the face, as shown in Figs 8b and c. It is also assumed that the support system applies a uniform pressure to the roof and floor and acts over a strip of width s.

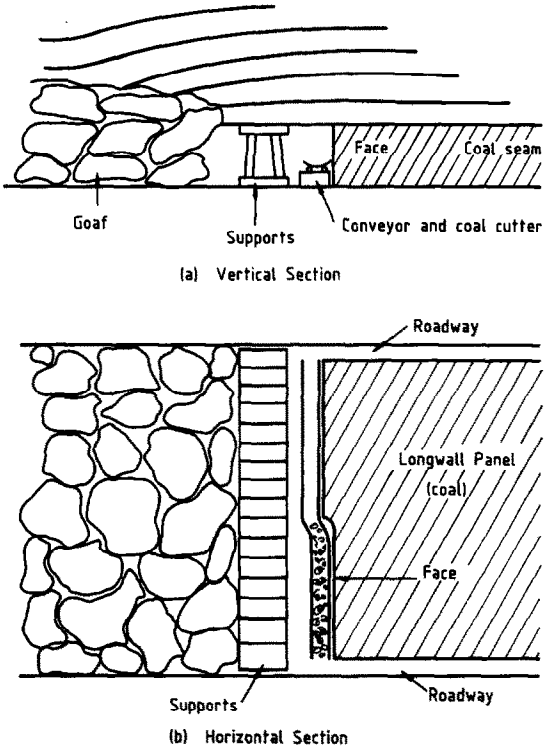

Fig. 7. Problem description.

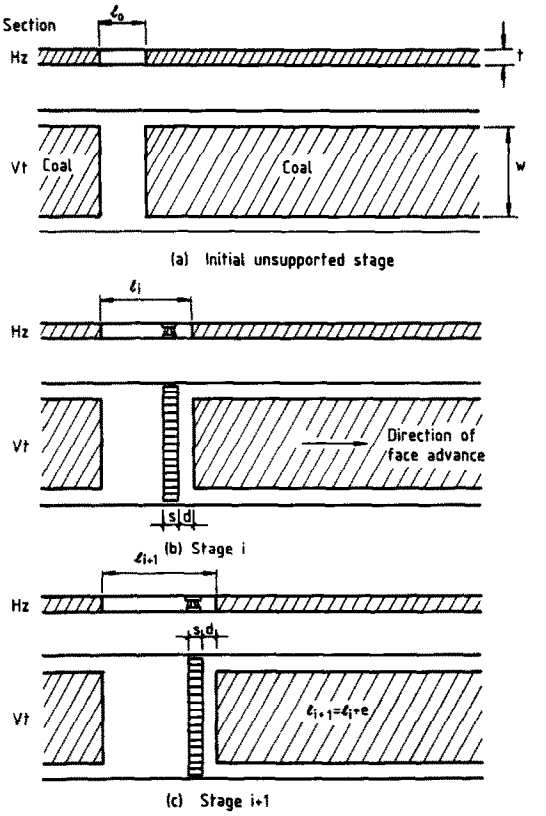

Fig. 8. Sequential excavation.

As a first approximation, it is assumed that the rock mass (including the coal) is homogeneous, isotropic and linearly elastic. Although this is probably the simplest model that might reasonably be used for the rock mass, it is a worthwhile exercise to pursue the implications of the structural interaction of such a continuum with the proposed support systems. To a first approximation the elastic model should reasonably predict the order of magnitude of the stresses and the displacements in the rock mass in the vicinity of the longwall face. This assertion should be valid because the rock immediately above, below and in front of the support system is restrained from undergoing gross, inelastic deformations by that very support. It is only behind the line of supports, i.e. in the goaf area, where large, inelastic movements (including caving) of the rock strata will occur. The effects that these large deformations may have on the interaction near the face might reasonably be incorporated in the analysis by adjusting the overall shape assumed for the goaf void and perhaps by allowing the transfer of some vertical load through caved material in the goaf.

In the analyses presented here it has been assumed that this void is rectangular in vertical section, as shown in Fig. 8, and that no transfer of vertical load occurs through caved material that collects in the "goaf" region.

In practice it is usual for the support system to be made up of a series of hydraulically powered jacks placed side by side along the longwall face. The structural model assumed for this system consists of a linear spring in series with a slider which has a finite compressive strength. The support system is assumed to apply a uniform pressure p to the roof and floor rocks over strips of width s, so that the total force applied to the roof and floor per unit length of the longwall face is $P = ps$. The spring has a stiffness k expressed in units of force per unit of axial displacement (compression) per unit length of the longwall face, i.e. k has the dimensions of stress. The spring yields and carries no further axial load, i.e. it compresses indefinitely, when the axial compressive force reaches a magnitude P_y also defined in units of force per unit length of the longwall face. The distance between the coal face and the edge of the supported strip of roof is denoted by the symbol d, as shown in Fig. 9.

Analysis

A specially formulated boundary element approach has been used to analyse this problem. However, the finite element technique could also be used.

Consider two successive stages in the excavation sequence, as depicted schematically in Fig. 10. At stage i, the support system is represented by a spring connecting nodes in the roof and floor at location i. At stage $i + 1$ the support spring has been moved in the same direction as the face advance and now connects roof and floor nodes at location $i + 1$.

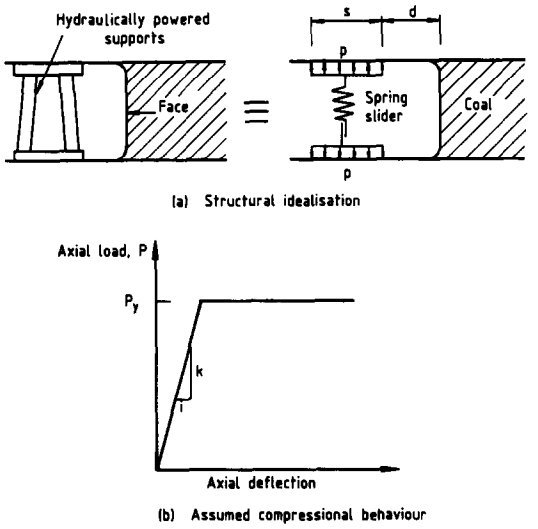

Fig. 9. Model of face support system.

Behaviour at stage i

The vertical displacements of the roof and floor nodes at location $i+1$ are given by

$$Er_{i,i+1} = \sigma_v A_{i,i+1} + p_i B_{i,i+1} \tag{7a}$$

$$Ef_{i,i+1} = \sigma_v C_{i,i+1} + p_i D_{i,i+1}. \tag{7b}$$

In the above equations a number of variables contain two subscripts: the first indicates the stage of excavation, while the second refers to the nodal location to which the quantity is applicable.

$(r, f)_{i,j}$ = vertical displacement of roof and floor nodes respectively.

$(A, C)_{i,j}$ = influence coefficients representing the contribution of the pre-mining stress field to the vertical displacements of roof and floor nodes respectively.

$(B, D)_{i,j}$ = influence coefficients representing the contribution of the support loading to the vertical displacements of roof and floor nodes respectively.

p_i = the applied support pressure at excavation stage i. For convenience this has been expressed in units of force per unit width of the support system per unit length of the longwall face. It may be thought of as the stress that the support system applies to the roof and floor of the opening in the neighbourhood of roof and floor nodes at location i.

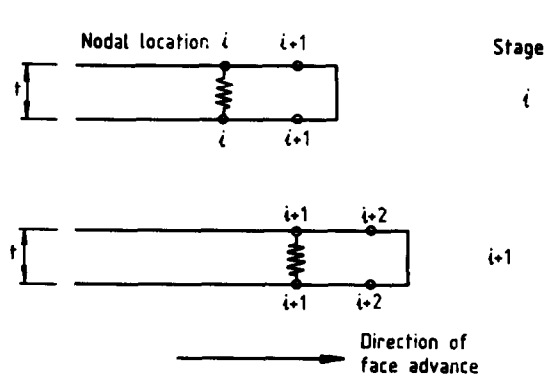

Fig. 10. Successive stages in excavation.

Also, σ_v denotes the magnitude of the vertical component of the pre-mining field stress and E is Young's modulus of the ideal, homogeneous, isotropic, elastic rock mass.

It is obvious that in eqn (7) the coefficients $A_{i,j}$, $B_{i,j}$, $C_{i,j}$ and $D_{i,j}$ all depend on the geometry of the opening and support system, the ratio of horizontal to vertical field stress, and Poisson's ratio of the homogeneous elastic rock mass.

The closure of the opening between roof and floor nodes at location $i+1$ at excavation stage i is given by

$$c_i = f_{i,i+1} - r_{i,i+1} = (C_{i,i+1} - A_{i,i+1})\sigma_v/E + (D_{i,i+1} - B_{i,i+1})p_i/E. \tag{8}$$

Incremental behaviour

Consider now the increment of excavation from stage i to $i+1$. The incremental closure between the nodes at location $i+1$ is

$$\begin{aligned}\Delta c &= c_{i+1} - c_i \\ &= (C_{i+1,i+1} - A_{i+1,i+1})\sigma_v/E \\ &\quad - (C_{i,i+1} - A_{i,i+1})\sigma_v/E \\ &\quad + (D_{i+1,i+1} - B_{i+1,i+1})p_{i+1}/E \\ &\quad - (D_{i,i+1} - B_{i,i+1})p_i/E.\end{aligned} \tag{9}$$

Support behaviour

Suppose that initially the support system can be represented by an elastic spring. Its stiffness relation, when expressed in terms of the stress p_{i+1} applied to the roof and floor at stage $i+1$, is given by

$$\Delta s = \left(\frac{p_{i+1}}{k}\right)t$$

where Δs is the shortening of the spring under the loading represented by p_{i+1}, and k is the spring stiffness, which in the present formulation has units of stress, i.e. it represents the force per unit length of the excavation face required to produce unit shortening of the support system and t is the height of the excavated void (=seam thickness).

We also allow the possibility for the support system to yield whenever $p_{i+1} = p_y$. Once yield has occurred at any stage in the excavation, the support system has zero incremental stiffness.

Interaction

(a) *Non-yielding, elastic support.* For this case the compatibility condition for the nodes at location $i+1$ requires that the closure of the opening is equal to the shortening of the support system, viz. $\Delta c = \Delta s$, which implies

$$\left(\frac{p_{i+1}}{E}\right) = \frac{F}{G} \tag{10}$$

where

$$F = (D_{i,i+1} - B_{i,i+1})p_i/E + (C_{i,i+1} - A_{i,i+1})\sigma_v/E - (C_{i+1,i+1} - A_{i+1,i+1})\sigma_v/E$$

$$G = D_{i+1,i+1} - B_{i+1,i+1} - Et/k$$

and

$$\Delta c = \Delta s = p_{i+1}/k. \tag{11}$$

(b) *Yielding supports.* When the support system yields the support pressure and the closure of the opening are given by

$$p_{i+1} = p_y \tag{12}$$

and

$$\Delta c = \Delta s = (C_{i+1,i+1} - A_{i+1,i+1})\sigma_v/E - (C_{i,i+1} - A_{i,i+1})\sigma_v/E + H \tag{13}$$

where

$$H = (D_{i+1,i+1} - B_{i+1,i+1})p_y/E - (D_{i,i+1} - B_{i,i+1})p_i/E.$$

Equations (10) and (13) are recurrence relations which can be used to analyse any given sequence of excavation stages where the support system follows the advance of the face, such as in longwall extraction of coal or other tabular ore bodies.

Typical results

Some typical results of this analysis are given in Figs 11 and 12. In determining these numerical results it was assumed that Poisson's ratio of the rock mass was 0.25 and the ratio of the pre-mining horizontal to vertical field stresses in the rock mass was 2.5. The geometric parameters are defined in Figs 11 and 12.

The variation of the support loading with width of extraction is shown in Fig. 12, where all quantities have been plotted non-dimensionally. The vertical axis shows values of the support pressure applied to the roof and floor normalized by the magnitude of the vertical component of the virgin field stress as well as the normalized force developed in the support system. The horizontal axis shows the width of the opening normalized by the seam thickness. Curves corresponding to selected values of the non-dimensional support stiffness k/E have been plotted; $k/E = \infty$ corresponds to the case of a completely rigid, unyielding support while $k/E = 0$ corresponds

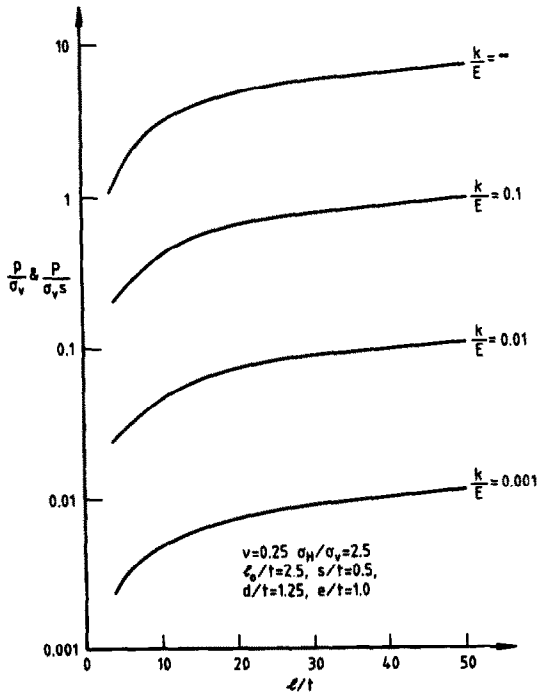

Fig. 11a. Variation of support loading—logarithmic scale.

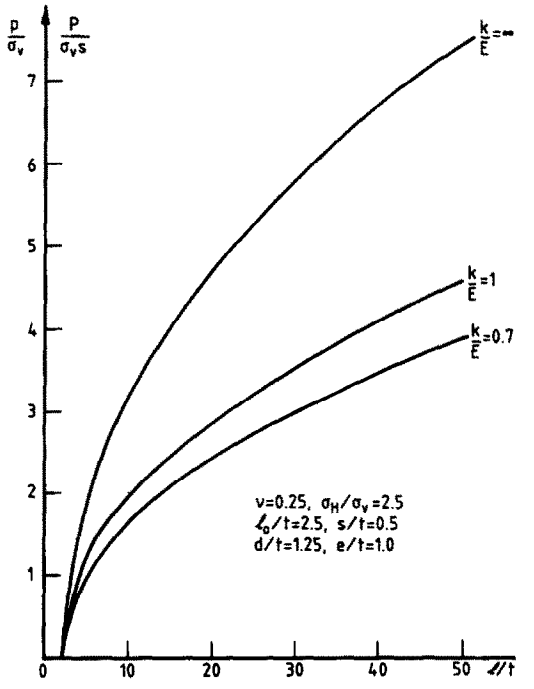

Fig. 11b. Variation of support loading—natural scale

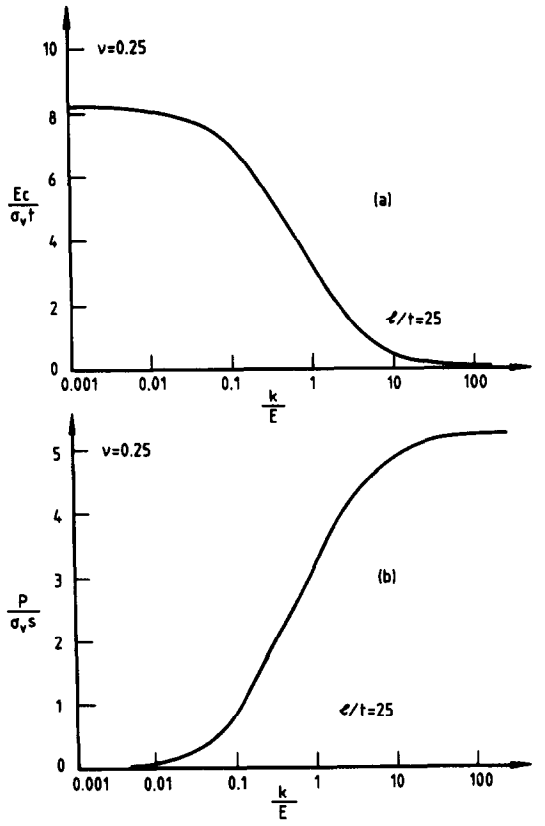

Fig. 12. Variation of closure and support load.

to no support at all. The results shown in Fig. 11a have been plotted using a logarithmic scale on the vertical axis to accommodate a wide range of values of k/E. In Fig. 11b a natural scale has been used on the vertical axis to provide greater detail for the cases where $k/E = \infty$, 1 and 0.7. It can be seen from these plots that in each case the load taken by the support system increases as the opening becomes wider (i.e. as the longwall face advances). The rate of increase is large at first but becomes more gradual at wider openings. The relative stiffness of the support system is important in determining the amount of load it will carry; the stiffer it is then the more load it attracts. This feature is also obvious in Fig. 12b where the load developed in the support system is plotted against the relative stiffness for the case where the excavation has reached a width given by $l/t = 25$. This figure shows that for values k/E less then about 0.01 the support system is almost totally ineffective in that it does not structurally interact with the surrounding rock mass and attract load. (A warning is given against interpreting the last statement too broadly; while the support system may undergo negligible structural interaction with the surrounding rock mass, in practice it may still be useful in providing support for fractured or caving rock immediately adjacent to the face. The latter type of behaviour is not considered here.) For values of k/E greater than about 10 the support system is effectively rigid and attracts the maximum vertical load, in this case given approximately by $P_{max} = 5.2\sigma_{vs}$.

In the case considered the support system has been treated as a simple elastic spring, i.e. it does not yield, and so the axial shortening of the support system c can always be calculated using the relation $c = pt/k$.

In Fig 12a the shortening of the support (i.e. the closure of the opening has been plotted non-dimensionally against the relative stiffness k/E for the case where $l/t = 25$. Again it may be seen that the support is structurally ineffective whenever $k/E < 0.01$ and it is effectively rigid whenever $k/E > 10$. In the former case the closure of the opening is the same as that calculated for an unsupported opening, while in the latter case there is no closure at the support point.

Analysis of pile foundations under cyclic loading

The design of pile foundations is a common problem for the geotechnical engineer, and many simplified techniques have been developed to analyse the behaviour of piles under simple loading conditions. However, a number of problems cannot properly be handled by simplified analyses, yet cannot economically be analysed by a full three-dimensional finite element analysis. An example is the behaviour of piles and groups subjected to cyclic loading, and for such a problem it is important to incorporate those elements of the behaviour of real soil which have an important effect on the response of the pile.

A very useful approach for this problem is to employ a form of boundary element analysis in which the pile is represented as an elastic cylinder and the surrounding soil mass as an elastic continuum. For static loading, the following factors are allowed for: pile–soil slip when the shear stress reaches the limiting value of shaft resistance, linear post-peak "softening" of the skin resistance to a residual value, a non-homogeneous soil profile, and interaction between piles in a group.

For cyclic loading, the following additional features are allowed for: cyclic degradation of shaft resistance, and bearing resistance, and soil Young's modulus, loading rate effects on the above parameters, and accumulation of permanent displacements under non-zero mean load.

A uniform-diameter pile can be discretized into a total of n elements, comprising cylindrical shaft elements and annular base elements, as shown in Fig. 13. The following equation can be derived from consideration of compatibility of incremental pile and soil vertical displacements:

$$[I/E_c - AD \cdot FE]\{\Delta p\} = \Delta\rho_b\{1\} = -\{\Delta S_p\} \quad (14)$$

in which

$[I/E_c] = n \times n$ matrix of soil influence factors determined from elastic theory [5], divided by E_c, the Young's modulus of the soil allowing for the effects of cyclic loading;

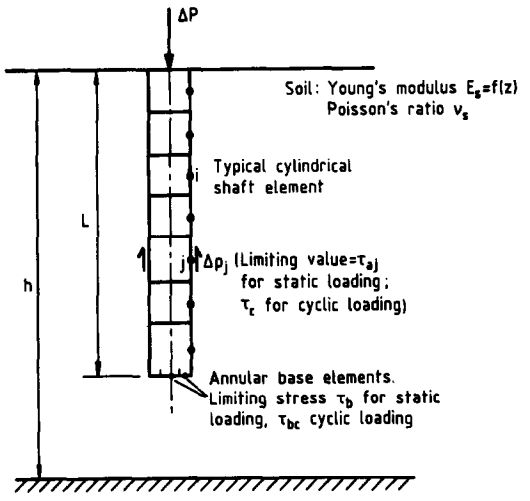

Fig. 13. Model of pile.

$[AD]$ = summation matrix $(n \times n)$;

$[FE]$ = pile compression matrix $(n \times n)$;

$\{\Delta p\}$ = vector of interaction stress increments;

$\{S_p\}$ = vector of incremental permanent soil displacement due to cyclic loading;

$\{\Delta \rho_b\}$ = incremental displacement of pile tip.

In addition, vertical equilibrium requires that:

$$\sum_{i=1}^{n} A_i \Delta p_i = \Delta P \tag{15}$$

where

A_i = surface area of element i

Δp_i = interaction stress increment on i

ΔP = increment of applied load on pile head.

Equations (14) and (15) provide sufficient equations to solve for the n unknown interaction stress increments Δp and the incremental displacement $\Delta \rho_b$ of the pile base. The total interaction stress p_i at an element i cannot exceed the limiting resistance τ_{ci} for that element, where τ_{ci} incorporates the effects of cyclic loading and loading rate. In the case of an element which exhibits strain-softening, τ_{ci} will be the smaller of the "strain-softened" static value of resistance and the cyclically degraded value of resistance. When p_i reaches the value τ_{ci}, the displacement compatibility equation for element i in eqn (14) is replaced by the condition

$$p_i = \tau_{ci} - p_{ii} \tag{16}$$

where p_{ii} = total pile–soil stress at previous load increment.

The solution is then recycled until, for all elements, the total pile–soil stress is less than or equal to the limiting value.

It should be noted that the analysis can be applied directly to symmetrical groups of piles in which all piles behave identically. In this case, the soil influence factors i in eqn (14) include the effects of all piles in the group.

When applying the above analysis to determine the response of a pile subjected to n cycles of uniform loading (maximum value P_{max}, minimum value P_{min}), the following procedure is employed:

(i) starting with static values of soil modulus and limiting pile–soil resistances (shaft and base) the pile is subjected to a load P_{max} and the response determined;
(ii) the load is decreased to P_{min} and the analysis is repeated. Finally, the load is returned to the mean load, completing the first cycle of loading;
(iii) the limiting pile–soil resistances and the soil Young's modulus are adjusted for cyclic loading effects, as described below;
(iv) the increment in permanent displacement, ΔS_p, for each element is determined (see below);
(v) steps (i)–(iv) are repeated for the next cycle, and the procedure repeated until all n cycles have been simulated.

If another sequence of cyclic loading, with different loads, is to be considered, the same procedure is followed, except that the starting values of limiting pile–soil resistance and soil Young's modulus are the values existing at the end of the previous sequence of loading. In this way, a complete "storm loading" analysis can be performed.

It should be noted that, in the case of a strain-softening interface, reduction of resistance at an element may occur due either to the effects of cyclic loading ("cyclic degradation") or to the effects of continued displacement beyond the point of peak static resistance ("static degradation"). The resistance used in the analysis is the lesser of the values from the two sources of degradation. When degradation of limiting shaft resistance in compression occurs due to strain-softening, it is assumed that the limiting shaft resistance in tension is also reduced to the same extent, and *vice versa*.

Application of the above analysis requires quantification of the effects of cyclic loading and loading rate on limiting shaft resistance, limiting base resistance, soil Young's modulus and permanent displacement of the pile. Tests on model piles in both silica sand and calcareous sand have revealed the following characteristics:

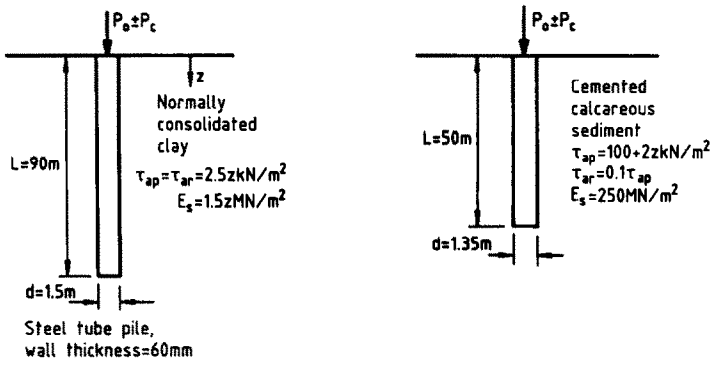

(a) Driven Offshore Steel Tube Pile in Normally Consolidated Clay

(b) Grouted Pile in Cemented Calcareous Sediment

Fig. 14. Hypothetical cases analysed.

(i) degradation of shaft resistance can be significant and appears to be related to the cyclic displacement which the shaft experiences. No degradation occurs until the cyclic displacement amplitude exceeds the displacement required to cause pile–soil slip under static loading. Thereafter, degradation occurs and is dependent on the number of cycles and the additional cyclic displacement;
(ii) degradation of limiting base resistance and soil Young's modulus is not significant;
(iii) loading rate effects are negligible in the sands tested;
(iv) the permanent displacements developed are a function of both the mean stress and cyclic stress levels and the number of cycles.

Using model test data in conjunction with the analysis described above, theoretical solutions have been obtained for a typical offshore pile subjected to cyclic axial loading. The problem is illustrated in Fig. 14 while Fig. 15 plots "fatigue curves" for the pile, relating the cyclic load level to the number of cycles to cause failure and the mean applied load level. In this case, it can be seen that, for normal mean load levels of the order of $0.2Q_c$ (where Q_c is the static ultimate compressive capacity of the pile), failure will not occur under cyclic loading unless the cyclic load exceeds about $0.43Q_c$. As the cyclic load level increases beyond that value, the number of cycles which can be sustained decreases.

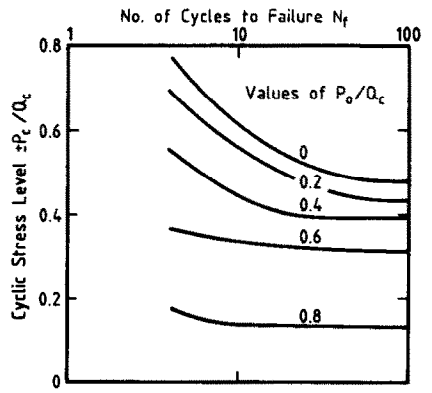

Fig. 15. Fatigue curves for driven pile-in clay.

Other information regarding the behaviour of the pile may also be obtained from such an analysis, e.g. the maximum displacement of the pile and its variation with number of cycles, the combinations of mean and cyclic load which result in no degradation, and the distribution of axial load along the pile and its variation during the cycling sequence.

Use of the finite element method to analyse such a problem would hardly have been feasible. It would have required the implementation of a constitutive model of soil behaviour which allowed for cyclic loading effects, an appropriate model of interface behaviour, and the simulation of hundreds or even thousands of cycles of loading with different combinations of mean and cyclic load. Such a task would be daunting, even with a super-computer. The boundary element techniques were, however, implemented with no difficulty on a modest capacity IBM personal computer.

CONCLUSIONS

The authors have discussed a number of examples in the geotechnical area which illustrate the necessity for the appropriate modelling of construction sequence and constitutive behaviour, and the desirability of using a suitably economic form of numerical analysis.

REFERENCES

1. J. T. Christian and I. H. Wong, Errors in simulating excavation in elastic media by finite elements. *Soils Fdns (Japan)* **13**, 1–10 (1973).
2. P. T. Brown and J. R. Booker, Finite element analysis of excavation. *Computers and Geotechnics* **1**, 207–220 (1985).
3. J. C. Small, *User Manual, Program FLEA, (Finite Layer Elastic Analysis)*. School of Civil and Mining Engineering, The University of Sydney (1986).

4. J. C. Small, *User Manual, Program FLAC (Finite Layer Analysis of Consolidation)*. School of Civil and Mining Engineering, The University of Sydney (1986).

5. H. G. Poulos and E. H. Davis, *Pile Foundation Analysis and Design*. John Wiley and Sons, New York (1980).